

Partially Interpenetrated NbO Topology Metal–Organic Framework Exhibiting Selective Gas Adsorption

Published as part of a *Crystal Growth and Design* virtual special issue on *Crystal Engineering of Nanoporous Materials for Gas Storage and Separation*

Gaurav Verma,[†] Sanjay Kumar,^{*,‡} Tony Pham,[†] Zheng Niu,[†] Lukasz Wojtas,[†] Jason A. Perman,^{*,†} Yu-Sheng Chen,[‡] and Shengqian Ma^{*,†}

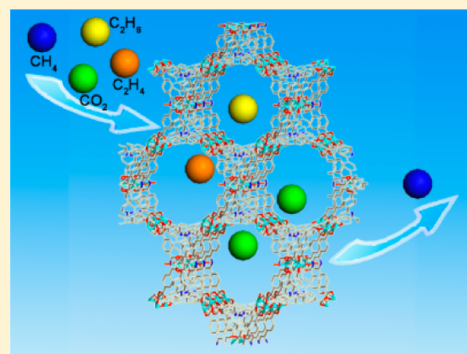
[†]Department of Chemistry, University of South Florida, 4202 East Fowler Avenue, Tampa, Florida 33620, United States

[‡]Department of Chemistry, Multani Mal Modi College, Patiala 147001, Punjab, India

[‡]ChemMatCARS, Center for Advanced Radiation Sources, The University of Chicago, 9700 South Cass Avenue, Argonne, Illinois 60439, United States

S Supporting Information

ABSTRACT: We report on the first partially interpenetrated metal–organic framework (MOF) with NbO topology for its ability to separate methane from carbon dioxide and permanently sequester the greenhouse gas CO₂. The MOF, Cu₂(pbpta) (H₄pbpta = 4,4',4'',4'''-(1,4-phenylenbis(pyridine-4,2,6-triyl))-tetrabenzoic acid), crystallizes in the monoclinic C2/m space group and has a 2537 m²/g Brunauer, Emmett and Teller surface area with an 1.06 cm³/g pore volume. The MOF exhibits selective adsorption of CO₂ over CH₄ as well as that of C₂H₆ and C₂H₄ over CH₄. Cu₂(pbpta) additionally shows excellent catalytic efficacy for the cycloaddition reaction of CO₂ with epoxides to produce industrially important cyclic carbonates using solvent-free conditions.



INTRODUCTION

Energy focus over the past decade has adjusted to explore and utilize natural gas from reserves and landfills because it remains competitive with cleaner energy alternatives. Methane, the primary component in natural gas and landfill gas, is many times fouled with other hydrocarbons and unwanted species such as CO₂, N₂, H₂S, and water. Production requires fuel enriching processes to remove unwanted gases primarily composed of CO₂. Cryogenic distillation and pressure swing adsorption (PSA) methods have been used for separating equal and unequal volumes of CH₄/CO₂ from landfills and wells.^{1,2} The distillation techniques suffer from high operating cost, while PSA techniques demand adsorbents with high CO₂ capacity and selectivity.^{3–5} Therefore, alternative methods are under development which show high separation capabilities to enrich methane. Furthermore, utilization of the CO₂ captured after methane enrichment needs attention as it can serve as a feedstock for various processes. Here, research efforts are devoted to enrich methane stocks and convert CO₂ into high-value added chemicals to truly remove it from the atmosphere and offset operational costs.

Beneficial catalysts that make use of CO₂ as the C₁ source are in dire need to replace expensive carbon capture and storage technologies. Numerous homogeneous catalysts using d⁸–d¹⁰ transitions metals have been shown to be useful in transforming

CO₂ into value-added chemicals.^{6,12} Whereas homogeneous catalysts offer many advantages, heterogeneous catalysts can be easily separated from the end products, thus offering the opportunity to continuously recycle the catalysts and offset initial costs. Where metals and metal nanoparticles participate as catalysts and cocatalysts, CO₂ diffusion to these active sites may require extreme conditions. This can be alleviated using porous materials with a high affinity for CO₂ at ambient conditions.⁷

Thus, in order to address the aforementioned issue of methane enrichment from CO₂ and utilize the captured CO₂ through transformation into industrially relevant products, multifunctional material platforms are needed. Many porous materials have been explored in this direction which can accomplish the task of both separation and acting as a catalyst to offset CO₂. These materials include zeolites, covalent organic frameworks (COFs), and metal–organic frameworks (MOFs).^{7–16}

MOFs are one of the most promising classes of porous materials due to their high surface area, tunable pore sizes and geometries, and accessible functionality sites, whereby they

Received: February 9, 2017

Revised: April 10, 2017

Published: April 10, 2017

continue to be useful for gas sorption, separation, and catalysis.^{17–20} Many MOFs exhibit high surface areas,^{21–23} but the large pores and void spaces are not necessarily useful for low pressure adsorption of CO₂. Therefore, techniques to reduce this free space and improve CO₂ adsorption at low pressure have been tested through postsynthetic modification on the ligands or metal clusters, and by interpenetration or catenation in the frameworks.^{24–28} Interpenetration is beneficial for many MOFs as shown with improvements in the material's robustness, stepwise gas adsorption, and selective adsorption.^{24,29} On a very rare instance, partial interpenetration has occurred in MOFs which can reduce the free space as observed in NOTT-202²⁹ and MUF-9.³⁰ This may not be as uncommon as traditionally thought as there is evidence of MOFs changing their degrees of interpenetration when induced by pressure and desolvation,^{26,31–35} whereby high quality X-ray diffraction techniques have been used to observe this phenomena. The selective adsorption of CO₂ is paramount for the development of various catalytic MOFs, which can actively participate in CO₂ transformation reactions to use it as a C₁ building block.^{36,37} Research efforts have found that CO₂ occupies a position near unsaturated metal centers (UMCs) in MOFs at low pressure.^{38–40} This high interaction between CO₂ and the UMC has led to high isosteric heats of adsorption (Q_{st}),^{36,41,42} which is useful for the development of various catalytic materials for CO₂ fixation reactions. Therefore, for the effective separation and fixation of CO₂, we synthesized Cu₂(pbpta), a partially interpenetrated MOF with NbO topology, examined its adsorption capabilities, and carried out cycloaddition reactions whereby the unsaturated Cu(II) actively participates in the formation of cyclic carbonates from solvent-free reactions.

EXPERIMENTAL SECTION

Materials and Methods. All reagents and solvents were purchased from commercial sources and used as received. Powder X-ray diffraction (PXRD) data were collected at room temperature using a Bruker D8 Advance theta-2theta diffractometer with copper radiation (Cu K α , $\lambda = 1.5406$ Å) and a secondary monochromator operating at 40 kV and 40 mA, whereby samples were measured between 3° and 50° at 0.5 s/step and step size of 0.05°. Single crystal X-ray diffraction data were collected using synchrotron radiation ($\lambda = 0.41328$ Å) at the Advanced Photon Source Beamline 15-ID-B of ChemMatCARS in Argonne National Lab, Argonne, IL. Infrared spectra measurements from 4000 to 400 cm⁻¹ were taken on a PerkinElmer FT-IR Spectrometer Spectrum Two (UATR Two) with 4 cm⁻¹ resolution. A TA Instruments TGA Q50 was used to record thermal gravimetric analysis (TGA) data from room temperature to 600 °C at a 10 °C/min rate. A Varian Unity Inova 400 spectrometer NMR was used to measure ¹H NMR. Gas adsorption measurements were performed using a Micromeritics ASAP 2020 surface area analyzer to collect N₂ (surface area measurement at 77 K), CO₂, CH₄, C₂H₆, and C₂H₄ isotherms at 273 and 298 K.

Synthesis of 2,6-Di-*p*-tolyl-4-(2,6-di-*p*-tolylpyin-4-yl)phenylpyridine. It was synthesized similarly as reported previously by Yang et al.⁴³ Yield: 78.6% ¹H NMR (CDCl₃, 400 MHz, ppm) δ : 2.46 (s, 12 H), 8.18 (d, 8 H), 7.95 (s, 8 H), 7.36 (d, 8 H).

Synthesis of 4,4',4'',4'''-(1,4-Phenylenebis(pyridine-4,2,6-triyl))-tetrabenzoic Acid (H₄pbpta). The reagent 2,6-di-*p*-tolyl-4-(2,6-di-*p*-tolylpyin-4-yl)-phenylpyridine (1.0 g, 1.69 mmol) was added slowly to HNO₃ (8 mL, 4 N) in a Teflon lined autoclave and heated to 180 °C for 48 h. After cooling, the reaction mixture was thoroughly washed with distilled water and purified by flash chromatography using an ethyl acetate/methanol (1/2 v/v) eluent. Yield: 74.2%, ¹H NMR (DMSO, 400 MHz, ppm) δ : 8.01 (d, 4 H), 8.11 (d, 8 H), 8.30 (s, 4 H), 8.46 (d, 8 H). FT-IR (cm⁻¹); $\nu = 3015$

(w, br.), 1682 (s), 1598 (m), 1573 (w), 1421 (m), 1280 (s), 1112 (m), 1015 (m), 861 (m), 775 (s), 728 (s).

Synthesis of Cu₂(pbpta). A mixture of the ligand H₄pbpta (7 mg, 0.01 mmol) and Cu(NO₃)₂·2.5H₂O (12 mg, 0.05 mmol) was dissolved in a 20 mL scintillation vial containing DMF (1.2 mL), EtOH (0.3 mL), and HNO₃ (80 μ L, 2.7 M). The reagents were sonicated in a sealed vial prior to being placed in an oven at 65 °C for 24 h to yield green parallelepiped crystals. Yield: 54.2%, FT-IR (cm⁻¹); $\nu = 3061$ (w, br.), 1593 (m), 1545 (m), 1383 (s), 1178 (w), 1104 (w), 1015 (m), 863 (w), 817 (m), 784 (s).

Cycloaddition Reactions of CO₂ with Epoxides. For a typical reaction, the oxide (25 mmol), Cu₂(pbpta) (20 mg equals 25 mmol of Cu(II)), and *n*-Bu₄NBr (0.58 g, 1.8 mmol) were added to a Schlenk tube and continuously purged with dry CO₂ at 1 atm while stirring at room temperature for 48 h. The progress of the reaction was monitored by ¹H NMR. This procedure was followed using the same molar amounts for propylene, epichlorohydrin, allyl glycidyl ether, and 1,2-butylene oxide. Control experiments were carried out without Cu₂(pbpta).

Ideal Adsorbed Solution Theory (IAST) Adsorption Selectivity. IAST adsorption selectivity was calculated following previously reported methods.⁴⁴ Single component adsorption isotherms (at room temperature) for each adsorbate were first fitted to the dual site Langmuir–Freundlich (DSLFF) model, and the obtained parameters were used to calculate the adsorption selectivity between two components. More details about the method and fitting parameters have been provided in the Supporting Information.

Estimation of Isosteric Heats of Adsorption, Q_{st} . At first, the adsorption data were fitted using the virial-type equation:⁴⁵

$$\ln p = \ln N + \left(\frac{1}{T}\right) \sum_{i=0}^m a_i N^i + \sum_j^n b_j N^j \quad (1)$$

Here p is the pressure expressed in Torr, N is the amount of adsorbed gas in mmol/g, T is the temperature in K, a_i and b_j are virial coefficients, and m , n represent the number of coefficients required to adequately describe the isotherms. Then the Clausius–Clapeyron eq 2 was

$$Q_{st} = RT^2 \left(\frac{\partial \ln p}{\partial T} \right)_q \quad (2)$$

employed to calculate the enthalpies of CO₂ adsorption. Combining eqs 1 and 2, the isosteric heat of adsorption can be calculated using the following equation:

$$Q_{st} = -R \sum_{i=0}^m a_i N^i \quad (3)$$

The fitting parameters of the virial model are given in Table S6, and the adsorption enthalpies (Q_{st}) with uptake are given in Figure Sd.

RESULTS AND DISCUSSION

Synthesis and Characterization. The molecule H₄pbpta is similar to ligands reported by Gole et al.,⁴⁶ Cai et al.,⁴⁷ and Alezi et al.,⁴⁸ which are extended analogues of the molecules used to construct the partially interpenetrated NOTT-202.²⁹ H₄pbpta (Figure 1) was synthesized in high yields from the oxidation of its methylated precursor.⁴³

A solvothermal reaction of Cu(NO₃)₂·2.5H₂O and H₄pbpta in a 5:1 molar ratio dissolved in an acidic mixture of ethanol/DMF (v/v = 1:4) heated at 65 °C for 24 h afforded single crystals of Cu₂(pbpta). The IR spectra of Cu₂(pbpta) shows the characteristic bands of coordinated carboxylate groups at 1593 and 1178 cm⁻¹ for asymmetric and symmetric stretches, respectively (Figure S1, Supporting Information). The asymmetric stretch is 89 cm⁻¹ red-shifted from the protonated reactant H₄pbpta.

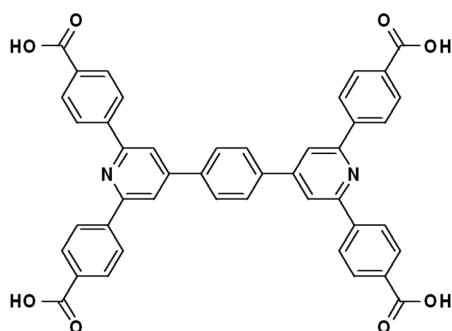


Figure 1. H_4pbpta ligand.

Crystal Structure Analysis. Block-shaped crystals suitable for single crystal X-ray diffraction experiments were harvested, and analyses found that $Cu_2(pbpta)$ crystallizes in the monoclinic $C2/m$ space group with a cell volume of 29547.9 \AA^3 . Unit cell parameters and structural factors are included in Table S1. The bulk phase of $Cu_2(pbpta)$ was confirmed by powder X-ray diffraction (Figure S2). The framework consists of two $Cu(II)$ centers arranged with four carboxylate ligands into a copper acetate motif or paddlewheel molecular building block (MBB) with water molecules coordinated in its axial positions. The average $Cu-Cu$ separation is $2.645 \pm 0.03 \text{ \AA}$, the carboxylate $Cu-O$ distance is $1.925 \pm 0.03 \text{ \AA}$, and the water $Cu-O$ distance is $2.132 \pm 0.21 \text{ \AA}$. Selected bond distances and angles of $Cu_2(pbpta)$ are listed in Tables S2 and S3. We give the molecular formula for the partially interpenetrated structure as $\{[Cu_2(pbpta)(2H_2O)] \cdot [Cu_2(pbpta)(2H_2O)]_{0.5} \cdot [Cu_2(pbpta)(2H_2O)]_{0.25}\}_n$, where the first framework (1) is fully occupied, and the latter two are 50% (2) and 25% (3) occupied, respectively, as determined by the occupancy factors from refinement of the crystal data. Partially interpenetrated frameworks 2 and 3 occupy similar but shifted positions in the crystal structure and can be considered disorder positions of each other. The second framework, from either 2 or 3, generates $2'$ or $3'$ from the space group's symmetry operations, which are unlikely to coexist because these symmetry related frameworks come within van der Waals distances as shown in Figure S4. Interpenetration from 1 with

either $2(2')$ or $3(3')$ is shown in Figure 2. Interactions from the interpenetration occur between the ligands of different frameworks where both $\pi-\pi$ and $CH-O$ are within the ranges of reported interactions⁴⁹ (Figure S3). The topological analysis of the fully occupied framework and the interpenetrating frameworks gives NbO topology (**nbo**) when considering both the MBB and the ligand as 4-connected nodes.

Physical Property Measurements. The as-synthesized and solvent exchanged $Cu_2(pbpta)$ displayed different thermograms from the TGA experiments. The as-synthesized material exhibited a near 50% mass loss up to $150 \text{ }^\circ\text{C}$ before it plateaued, whereas methanol exchanged $Cu_2(pbpta)$ only lost 10% in mass, which can be accounted for by 2.5 molecules of methanol per molecular unit (without interpenetration), before the material began to decompose near $250 \text{ }^\circ\text{C}$ (Figure S5, Supporting Information). The material could not be directly activated for gas adsorption experiments by methanol exchange and evacuation. It required an additional exchange with liquid CO_2 before it was supercritically dried and then placed on an ASAP 2020 outgas port at $80 \text{ }^\circ\text{C}$ for 10 h at a pressure lower than $10 \text{ } \mu\text{m Hg}$. A nitrogen adsorption-desorption isotherm at 77 K was collected for $Cu_2(pbpta)$ and resulted in a Type I adsorption profile, which indicates characteristics of microporous materials (Figure 3). The calculated Brunauer, Emmett and Teller (BET) accessible surface area and total pore volume were $2537 \text{ m}^2/\text{g}$ and $1.06 \text{ cm}^3/\text{g}$, respectively. Pore size distribution was evaluated using the density functional theory model and found pores of width less than 15 \AA . This value agrees well with pore size measurements from the crystal structure.

Natural Gas Adsorption Experiments. Low pressure gas adsorption experiments with components of natural gas were carried out on $Cu_2(pbpta)$ at 273 and 298 K up to 810 mmHg of pressure. The isotherms are shown in Figure 4, and the maximum uptake capacities are listed in Table 1. From these data we were able to calculate the Q_{st} at zero and higher loadings using the virial method (Figure Sd). We observe that $Cu_2(pbpta)$ preferentially adsorbs more CO_2 , ethane, and ethylene than CH_4 . This is also reflected in the calculated Q_{st} values showing lower methane values at all loading concentrations. As shown in Table 2, the high Q_{st} of CO_2 at zero

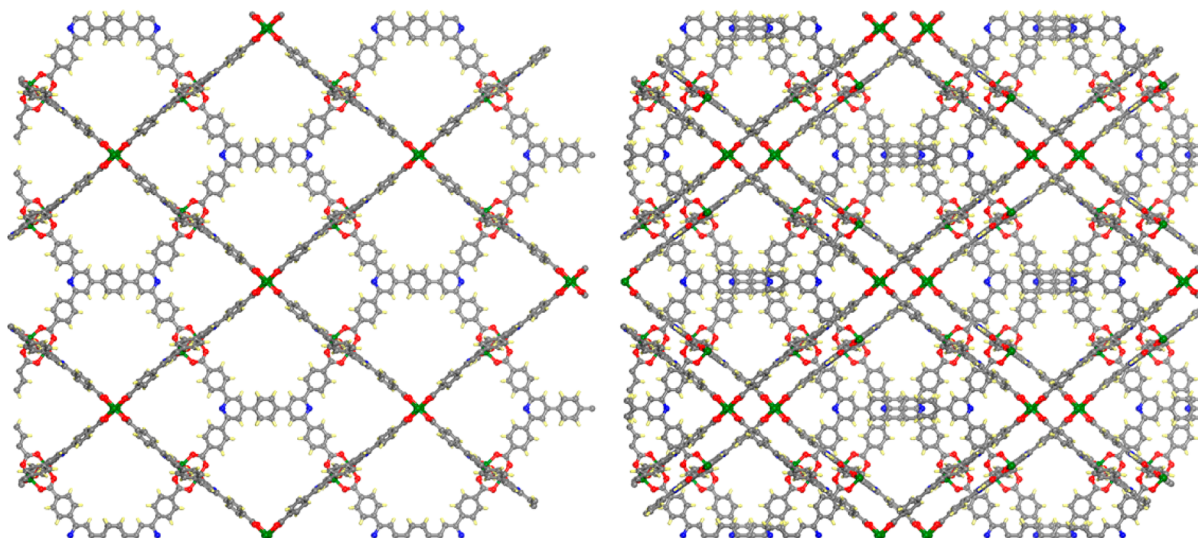


Figure 2. Non-interpenetrated and interpenetrated view along the z -axis.

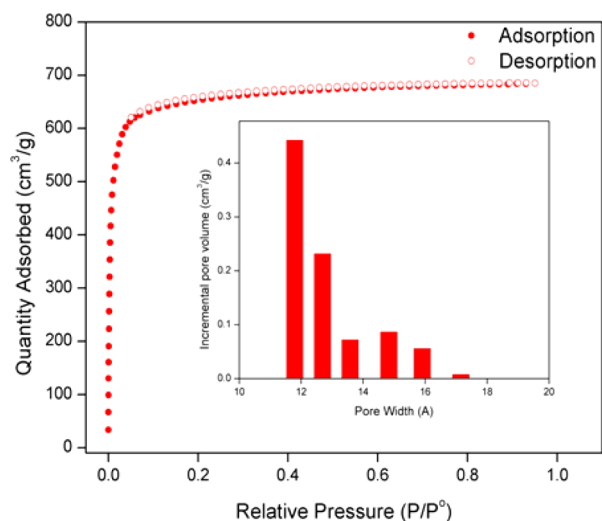


Figure 3. Nitrogen adsorption–desorption isotherm at 77 K. Inset shows the pore size distribution.

loading of 27 kJ/mol in $\text{Cu}_2(\text{pbpta})$ is higher than MOF-5 (17 kJ/mol),⁵⁰ UCMC-1 (12 kJ/mol),⁵¹ CuBTTri (21 kJ/mol),⁵² and ZJNU-54a (24.7 kJ/mol)⁵³ but comparable to JUC-199 (29 kJ/mol),⁵⁴ HKUST-1 (hydrated) (30 kJ/mol),⁵⁵ and MIL-53(Cr) (32 kJ/mol).⁵⁶ We attribute this high value of the heat of adsorption to the presence of unsaturated metal centers (UMCs) in the framework which show strong interactions with

Table 1. Uptake Capacities (in mmol/g) for Different Gases at 273 and 298 K

	CO_2	CH_4	C_2H_4	C_2H_6
273 K	3.30	0.73	2.46	3.16
298 K	1.88	0.56	2.14	2.44

the quadrupole of CO_2 ⁵⁷ and a likely second interaction with the ligand's pyridyl nitrogen atom, which possesses a lone pair of electrons.⁵⁸

To establish the separation capability of CO_2 over methane, the adsorption selectivity was determined using IAST calculations. The selectivity was estimated as a function of pressure at 298 K under 101 kPa at an equimolar composition, a general landfill gas feed composition for a CO_2/CH_4 mixture. The selectivity at 298 K was also determined for an equimolar (50:50) and an excess (1:99) composition for the $\text{CO}_2/\text{C}_2\text{H}_4$ and $\text{CO}_2/\text{C}_2\text{H}_6$ mixtures. As shown in Figure 5a, the adsorption selectivity for the CO_2/CH_4 increases with an increase in total pressure and reaches an adsorption selectivity value of ~ 6 , which is higher than many reported MOFs under same conditions and comparable to JUC-199 (~ 9) previously reported.⁵⁴ The selectivity at 273 K for an equimolar mixture reaches ~ 11 and is ~ 8 for a 1:99 mixture of the two gases. The selectivity for an equimolar $\text{C}_2\text{H}_4/\text{CH}_4$ mixture is ~ 12 and for $\text{C}_2\text{H}_6/\text{CH}_4$ mixture is ~ 15 at 298 K, which is higher than FIR-7a-ht⁵⁹ (~ 8.6 for $\text{C}_2\text{H}_4/\text{CH}_4$ mixture and ~ 14.6 and for $\text{C}_2\text{H}_6/\text{CH}_4$

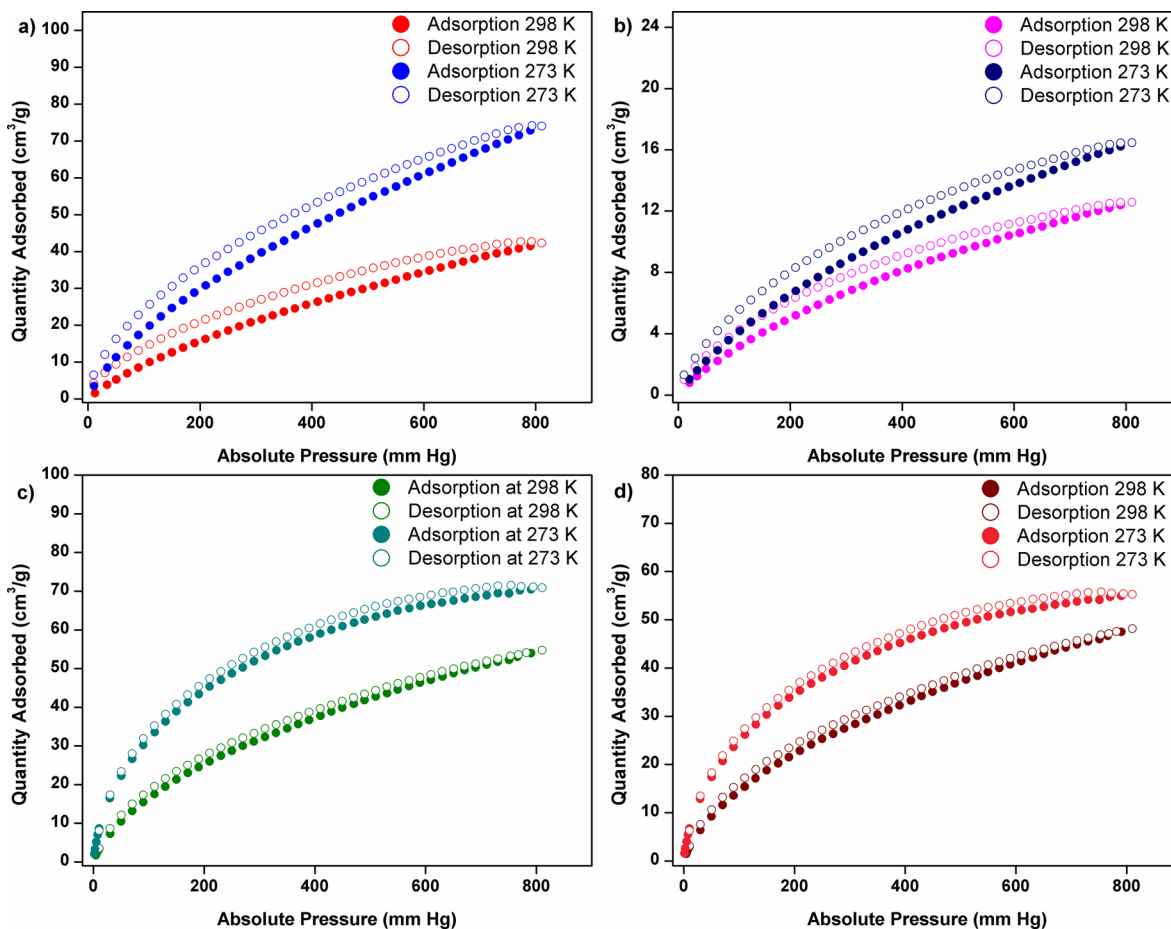


Figure 4. Adsorption–desorption isotherms at 273 and 298 K for (a) CO_2 , (b) CH_4 , (c) C_2H_6 , and (d) C_2H_4 .

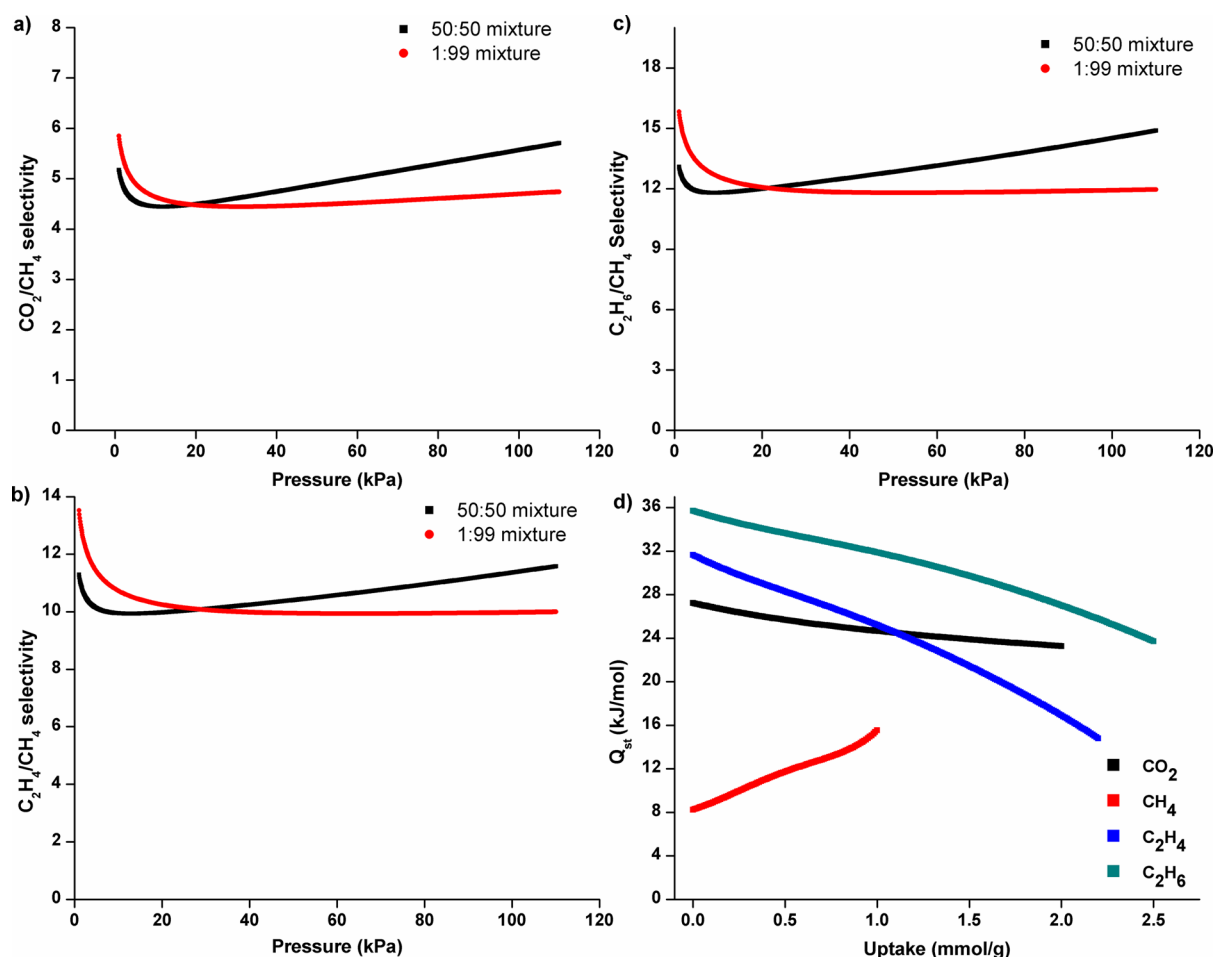


Figure 5. IAST adsorption selectivity at 298 K of equimolar (50:50) and excess (1:99) ratios for (a) $\text{CO}_2/\text{C}_2\text{H}_4$, (b) $\text{C}_2\text{H}_4/\text{CH}_4$, (c) $\text{C}_2\text{H}_6/\text{CH}_4$, and (d) Q_{st} for CO_2 , CH_4 , C_2H_4 , and C_2H_6 .

Table 2. Q_{st} values (in kJ/mol) for CO_2 for Different Materials at Zero Loading

	MOF-5 ⁵⁰	UMCM-1 ⁵¹	CuBTTri ⁵²	ZJNU-54a ⁵³	JUC-199 ⁵⁴	MIL-53(Cr) ⁵⁵	HKUST-1 (hydrated) ⁵⁶	$\text{Cu}_2(\text{pbpta})$
Q_{st} (kJ/mol)	17	12	21	24.7	29	32	30	27

mixture at 1 bar and 298 K), MFM-202a⁶⁰ (~ 8 for $\text{C}_2\text{H}_4/\text{CH}_4$ mixture and ~ 10 and for $\text{C}_2\text{H}_6/\text{CH}_4$ mixture at 1 bar and 293 K) and comparable to UTSA-35a⁶¹ (~ 10 for $\text{C}_2\text{H}_4/\text{CH}_4$ mixture and ~ 20 for $\text{C}_2\text{H}_6/\text{CH}_4$ mixture at 1 bar and 296 K). The selectivity values at 273 K for equimolar and excess (1:99) mixtures for these gases are provided in Figures S6–S8 in Supporting Information. The Q_{st} values at 1.0 mmol/g of gas was realized at 32, 25, and 16 kJ/mol, respectively, for C_2H_6 , C_2H_4 , and CH_4 . Again, these values are similar to MMF-202a and UTSA-35a at low coverage.^{60,61} The high selectivity values are in accordance with the adsorption isotherms for the single components and Q_{st} values. These results suggest that $\text{Cu}_2(\text{pbpta})$ is an efficient material for capture and effective separation of CO_2 from methane.

Cycloaddition of CO_2 with Epoxide. Since it is likely that CO_2 will be trapped in $\text{Cu}_2(\text{pbpta})$ after enriching methane, the presence of unsaturated metal centers have an added benefit to allow for selective heterogeneous catalysis of CO_2 into value-added chemicals. Several MOFs have been employed as Lewis acid catalysts for the chemical conversion of CO_2 with other reagents, but these reactions require demanding conditions, such as high pressure and high temperature.^{62–65} We have

followed previous procedures to convert epoxides¹¹ (Scheme 1) into cyclic carbonates using CO_2 and present our results in

Scheme 1. General Reaction Scheme for Conversion of Epoxides to Corresponding Cyclic Carbonates

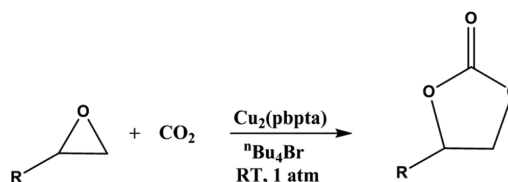

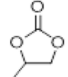
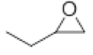
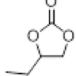
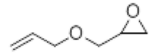
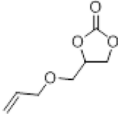

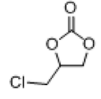


Table 3. The $\text{Cu}_2(\text{pbpta})$ showed a very high catalytic efficiency for the cycloaddition of epichlorohydrin to form epichlorohydrin carbonate in 94.3% yield after 48 h. Also, for the conversion of propylene oxide to propylene carbonate, the yield was 89.8% after 48 h, comparable to that of various porous materials reported before.^{66–72,11,16} High catalytic activity was also observed for the conversion of other epoxides to form their corresponding carbonates in quantitative yield (Table 3) at ambient temperature over a 48 h period. A decrease in product

Table 3. Cu-pbpta Catalyzed Addition of CO₂ and Epoxide

Cu-pbpta catalyzed addition of CO ₂ and epoxide			
Entry	Epoxide	Product ^[a]	Yield (%)
1			89.8
2			82.1
3			74.5
4			94.3

^aReaction conditions: epoxide (25 mmol), Cu-pbpta (20 mg), *n*-Bu₄NBr (0.58g), RT, CO₂ (1 atm pressure), 48 h.

yield was observed when the epoxide reagent's size was increased, and we attributed this decrease to slower diffusion of the analytes into the MOF through its fixed apertures.

CONCLUSION

In summary, we synthesized Cu₂(pbpta), the first case reported for a partially interpenetrated MOF exhibiting NbO topology. The solvothermal reaction was suitable to reproduce the partially interpenetrated material as observed by single crystal and powder X-ray diffraction studies. The Cu₂(pbpta) exhibits a high surface area of 2537 m²/g and adsorption selectivity for CO₂, ethane, and ethylene over methane. In addition, due to presence of high density of catalytically active sites, it serves as a highly efficient catalyst for conversion of CO₂ into cyclic carbonates at ambient conditions. Further work to understand the partial interpenetration of this MOF is under investigation.

ASSOCIATED CONTENT

Supporting Information

The Supporting Information is available free of charge on the ACS Publications website at DOI: 10.1021/acs.cgd.7b00198.

Powder X-ray diffraction patterns, TGA curves, crystallographic tables (PDF)

Accession Codes

CCDC 1531622 contains the supplementary crystallographic data for this paper. These data can be obtained free of charge via www.ccdc.cam.ac.uk/data_request/cif, or by emailing data_request@ccdc.cam.ac.uk, or by contacting The Cambridge Crystallographic Data Centre, 12 Union Road, Cambridge CB2 1EZ, UK; fax: +44 1223 336033.

AUTHOR INFORMATION

Corresponding Authors

*E-mail: sqma@usf.edu (S.M.).

*E-mail: sanjay2002@gmail.com (S.K.).

*E-mail: perman@usf.edu (J.A.P.).

ORCID

Jason A. Perman: 0000-0003-4894-3561

Shengqian Ma: 0000-0002-1897-7069

Notes

The authors declare no competing financial interest.

ACKNOWLEDGMENTS

The authors acknowledge the National Science Foundation (DMR-1352065) and the University of South Florida (USF) for financial support of this work. S.K. acknowledges the financial support from the University Grants Commission (UGC), New Delhi, India (No. F 5-80/2014(IC)). Chem-MatCARS Sector 15 is principally supported by the Divisions of Chemistry (CHE) and Materials Research (DMR), National Science Foundation, under Grant Number NSF/CHE-1346572. Use of the Advanced Photon Source, an Office of Science User Facility operated for the U.S. Department of Energy (DOE) Office of Science by Argonne National Laboratory, was supported by the U.S. DOE under Contract No. DE-AC02-06CH11357.

REFERENCES

- D'Alessandro, D. M.; Smit, B.; Long, J. R. *Angew. Chem., Int. Ed.* **2010**, *49*, 6058–6082.
- Cavenati, S.; Grande, C. A.; Rodrigues, A. E. *Energy Fuels* **2006**, *20*, 2648–2659.
- Pirngruber, G. D.; Hamon, L.; Bourrelly, S.; Llewellyn, P. L.; Lenoir, E.; Guillerm, V.; Serre, C.; Devic, T. *ChemSusChem* **2012**, *5*, 762–776.
- Yang, R. T. *Adsorbents: Fundamentals and Applications*; John Wiley & Sons Inc.: Hoboken, 2003.
- Kong, L.; Zou, R.; Bi, W.; Zhong, R.; Mu, W.; Liu, J.; Han, R. P. S.; Zou, R. *J. Mater. Chem. A* **2014**, *2*, 17771–17778.
- Cokoja, M.; Bruckmeier, C.; Rieger, B.; Herrmann, W. A.; Kühn, F. E. *Angew. Chem., Int. Ed.* **2011**, *50*, 8510–853.
- Sneddon, G.; Greenaway, A.; Yiu, H. H. P. *Adv. Energy Mater.* **2014**, *4*, 1301873.
- Xie, Y.; Wang, T.-T.; Liu, X.-H.; Zou, K.; Deng, W.-Q. *Nat. Commun.* **2013**, *4*, 1960.
- Zhang, G.; Wei, G.; Liu, Z.; Oliver, S. R. J.; Fei, H. *Chem. Mater.* **2016**, *28*, 6276–6281.
- Yang, D.-A.; Cho, H.-Y.; Kim, J.; Yang, S.-T.; Ahn, W.-S. *Energy Environ. Sci.* **2012**, *5*, 6465–6473.
- Kumar, S.; Wani, M. Y.; Arranja, C. T.; e Silva, J. de A.; Avula, B.; Sobral, A. J. F. N. *J. Mater. Chem. A* **2015**, *3*, 19615–19637.
- He, H.; Perman, J. A.; Zhu, G.; Ma, S. *Small* **2016**, *12*, 6309–6324.

- (13) Lin, S.; Diercks, C. S.; Zhang, Y.-B.; Kornienko, N.; Nichols, E. M.; Zhao, Y.; Paris, A. R.; Kim, D.; Yang, P.; Yaghi, O. M.; Chang, C. J. *Science* **2015**, *349*, 1208–1213.
- (14) Bae, Y.-S.; Mulfort, K. L.; Frost, H.; Ryan, P.; Punnathanam, S.; Broadbelt, L. J.; Hupp, J. T.; Snurr, R. Q. *Langmuir* **2008**, *24*, 8592–8598.
- (15) McEwen, J.; Hayman, J. D.; Yazaydin, A. O. *Chem. Phys.* **2013**, *412*, 72–76.
- (16) Sun, Q.; Jin, Y.; Aguila, B.; Meng, X.; Ma, S.; Xiao, F.-S. *ChemSusChem* **2017**, *10*, 1160–1165.
- (17) Li, B.; Chrzanowski, M.; Zhang, Y.; Ma, S. *Coord. Chem. Rev.* **2016**, *307*, 106–129.
- (18) Lu, W.; Wei, Z.; Gu, Z.-Y.; Liu, T.-F.; Park, J.; Park, J.; Tian, J.; Zhang, M.; Zhang, Q.; Gentle, T., III; Bosch, M.; Zhou, H.-C. *Chem. Soc. Rev.* **2014**, *43*, 5561–5593.
- (19) Zhang, M.; Bosch, M.; Gentle, T., III; Zhou, H.-C. *CrystEngComm* **2014**, *16*, 4069–4083.
- (20) Furukawa, H.; Cordova, K. E.; O’Keeffe, M.; Yaghi, O. M. *Science* **2013**, *341*, 1230444.
- (21) Zheng, B. S.; Bai, J. F.; Duan, J. G.; Wojtas, L.; Zaworotko, M. J. *J. Am. Chem. Soc.* **2011**, *133*, 748–751.
- (22) Eubank, J. F.; Nouar, F.; Luebke, R.; Cairns, A. J.; Wojtas, L.; Alkordi, M.; Bousquet, T.; Hight, M. R.; Eckert, J.; Embs, J. P.; Georgiev, P. A.; Eddaoudi, M. *Angew. Chem., Int. Ed.* **2012**, *51*, 10099–10103.
- (23) O’Keeffe, M.; Yaghi, O. M. *Chem. Rev.* **2012**, *112*, 675–702.
- (24) Jiang, H.-L.; Makal, T. A.; Zhou, H.-C. *Coord. Chem. Rev.* **2013**, *257*, 2232–2249.
- (25) Han, S. S.; Jung, D.-H.; Heo, J. *J. Phys. Chem. C* **2013**, *117*, 71–77.
- (26) Aggarwal, H.; Das, R. K.; Bhatt, P. M.; Barbour, L. J. *Chem. Sci.* **2015**, *6*, 4986–4992.
- (27) Gong, Y.-N.; Zhong, D.-C.; Lu, T.-B. *CrystEngComm* **2016**, *18*, 2596–2606.
- (28) Ma, S.; Sun, D.; Ambrogio, M.; Fillinger, J. A.; Parkin, S.; Zhou, H.-C. *J. Am. Chem. Soc.* **2007**, *129*, 1858–1859.
- (29) Yang, S.; Lin, X.; Lewis, W.; Suyetin, M.; Bichoutskaia, E.; Parker, J. E.; Tang, C. C.; Allan, D. R.; Rizkallah, P. J.; Hubberstey, P.; Champness, N. R.; Thomas, K. M.; Blake, A. J.; Schröder, M. *Nat. Mater.* **2012**, *11*, 710–716.
- (30) Ferguson, A.; Liu, L.; Tapperwijn, S. J.; Perl, D.; Coudert, F.-X.; Van Cleuvenbergen, S.; Verbiest, T.; van der Veen, M. A.; Telfer, S. G. *Nat. Chem.* **2016**, *8*, 250–257.
- (31) Aggarwal, H.; Lama, P.; Barbour, L. J. *Chem. Commun.* **2014**, *50*, 14543–14546.
- (32) Aggarwal, H.; Bhatt, P. M.; Bezuidenhout, C. X.; Barbour, L. J. *J. Am. Chem. Soc.* **2014**, *136*, 3776–3779.
- (33) Choi, S. B.; et al. *Angew. Chem., Int. Ed.* **2012**, *51*, 8791–8795.
- (34) Zhang, J.-P.; Lin, Y.-Y.; Zhang, W.-X.; Chen, X.-M. *J. Am. Chem. Soc.* **2005**, *127*, 14162–14163.
- (35) Lapidus, S. H.; Halder, G. J.; Chupas, P. J.; Chapman, K. W. *J. Am. Chem. Soc.* **2013**, *135*, 7621–7628.
- (36) Beyzavi, M. H.; Stephenson, C. J.; Liu, Y.; Karagiari, O.; Hupp, J. T.; Farha, O. K. *Front. Energy Res.* **2015**, *2*, 63.
- (37) Sumida, K.; Rogow, D.; Mason, J. A.; McDonald, T. M.; Bloch, E. D.; Herm, Z. R.; Bae, T.-H.; Long, J. R. *Chem. Rev.* **2012**, *112*, 724–781.
- (38) Scott, H. S.; Ogiwara, N.; Chen, K.-J.; Madden, D. G.; Pham, T.; Forrest, K.; Space, B.; Horike, S.; Perry, J. J., IV; Kitagawa, S.; Zaworotko, M. J. *Chem. Sci.* **2016**, *7*, 5470–5476.
- (39) Pham, T.; Forrest, K. A.; Chen, K.-J.; Kumar, A.; Zaworotko, M. J.; Space, B. *Langmuir* **2016**, *32*, 11492–11505.
- (40) Das, A.; D’Alessandro, D. M. *CrystEngComm* **2015**, *17*, 706–718.
- (41) Collins, S. P.; Daff, T. D.; Piotrkowski, S. S.; Woo, T. K. *Sci. Adv.* **2016**, *2*, e1600954.
- (42) Wilmer, C. E.; Leaf, M.; Lee, C. Y.; Farha, O. K.; Hauser, B. G.; Hupp, J. T.; Snurr, R. Q. *Nat. Chem.* **2011**, *4*, 83–89.
- (43) Yang, J.-X.; Tao, X.-T.; Yuan, C. X.; Yan, Y. X.; Wang, L.; Liu, Z.; Ren, Y.; Jiang, M. H. *J. Am. Chem. Soc.* **2005**, *127*, 3278–3279.
- (44) Li, B.; Zhang, Y.; Krishna, R.; Yao, K.; Han, Y.; Wu, Z.; Ma, D.; Shi, Z.; Pham, T.; Space, B.; Liu, J.; Thallapally, P. K.; Liu, J.; Chrzanowski, M.; Ma, S. *J. Am. Chem. Soc.* **2014**, *136*, 8654–8660.
- (45) Dincă, M.; Dailly, A.; Liu, Y.; Brown, C. M.; Neumann, D. A.; Long, J. R. *J. Am. Chem. Soc.* **2006**, *128*, 16876–16883.
- (46) Gole, B.; Bar, A. K.; Mallick, A.; Banerjee, R.; Mukherjee, P. S. *Chem. Commun.* **2013**, *49*, 7439–7441.
- (47) Cai, J.; Yu, J.; Wang, H.; Duan, X.; Zhang, Q.; Wu, C.; Cui, Y.; Yu, Y.; Wang, Z.; Chen, B.; Qian, G. *Cryst. Growth Des.* **2015**, *15*, 4071–4074.
- (48) Alezi, D.; Belmabkhout, Y.; Suyetin, M.; Bhatt, P. M.; Weseliński, L. J.; Solovyeva, V.; Adil, K.; Spanopoulos, L.; Trikalitis, P. N.; Emwas, A.-H.; Eddaoudi, M. *J. Am. Chem. Soc.* **2015**, *137*, 13308–13318.
- (49) Desiraju, G. R.; Steiner, T. *The Weak Hydrogen Bond: In Structural Chemistry and Biology*; Oxford University Press, 2001.
- (50) Choi, J.-S.; Son, W.-J.; Kim, J.; Ahn, W.-S. *Microporous Mesoporous Mater.* **2008**, *116*, 727–731.
- (51) Mu, B.; Schoenecker, P. M.; Walton, K. S. *J. Phys. Chem. C* **2010**, *114*, 6464–6471.
- (52) Demessence, A. D.; D’Alessandro, M.; Foo, M. L.; Long, J. R. *J. Am. Chem. Soc.* **2009**, *131*, 8784–8786.
- (53) Jiao, J.; Dou, L.; Liu, H.; Chen, F.; Bai, D.; Feng, Y.; Xiong, S.; Chen, D.-L.; He, Y. *Dalton Trans.* **2016**, *45*, 13373–13382.
- (54) He, H.; Sun, F.; Aguila, B.; Perman, J. A.; Ma, S.; Zhu, G. *J. Mater. Chem. A* **2016**, *4*, 15240–15246.
- (55) Liang, Z.; Marshall, M.; Chaffee, A. L. *Energy Procedia* **2009**, *1*, 1265–1271.
- (56) Bourrelly, S.; Llewellyn, P. L.; Serre, C.; Millange, F.; Loiseau, T.; Férey, G. *J. Am. Chem. Soc.* **2005**, *127*, 13519–13521.
- (57) Liu, D.; Zhong, C. *J. Mater. Chem.* **2010**, *20*, 10308–10318.
- (58) Wang, X.-J.; Li, P.-Z.; Chen, Y.; Zhang, Q.; Zhang, H.; Chan, X. X.; Ganguly, R.; Li, Y.; Jiang, J.; Zhao, Y. *Sci. Rep.* **2013**, *3*, 1149.
- (59) He, Y.-P.; Tan, Y.-X.; Zhang, J. *Chem. Commun.* **2013**, *49*, 11323–11325.
- (60) Gao, S.; Morris, C. G.; Lu, Z.; Yan, Y.; Godfrey, H. G. W.; Murray, C.; Tang, C. C.; Thomas, K. M.; Yang, S.; Schröder, M. *Chem. Mater.* **2016**, *28*, 2331–2340.
- (61) He, Y.; Zhang, Z.; Xiang, S.; Fronczek, F. R.; Krishna, R.; Chen, B. *Chem. Commun.* **2012**, *48*, 6493–6495.
- (62) Phan, A.; Doonan, C. J.; Uribe-Romo, F. J.; Knobler, C. B.; O’Keeffe, M.; Yaghi, O. M. *Acc. Chem. Res.* **2010**, *43*, 58–67.
- (63) Yano, T.; Matsui, H.; Koike, T.; Ishiguro, H.; Fujihara, H.; Yoshihara, M.; Maeshima, T. *Chem. Commun.* **1997**, 1129–1130.
- (64) Srivastava, R.; Srinivas, D.; Ratnasamy, P. *J. Catal.* **2005**, *233*, 1–15.
- (65) Chun, J.; Kang, S.; Kang, N.; Lee, S. M.; Kim, H. J.; Son, S. U. *J. Mater. Chem. A* **2013**, *1*, 5517–5523.
- (66) Kleist, W.; Jutz, F.; Maciejewski, M.; Baiker, A. *Eur. J. Inorg. Chem.* **2009**, *2009*, 3552–3561.
- (67) Zhou, Z.; He, C.; Xiu, J.; Yang, L.; Duan, C. *J. Am. Chem. Soc.* **2015**, *137*, 15066–15069.
- (68) Han, Y.-H.; Zhou, Z.-Y.; Tian, C.-B.; Du, S.-W. *Green Chem.* **2016**, *18*, 4086–4091.
- (69) Gao, W.-Y.; Chen, Y.; Niu, Williams, K.; Cash, L.; Perez, P. J.; Wojtas, L.; Cai, J.; Chen, Y.-S.; Ma, S. *Angew. Chem., Int. Ed.* **2014**, *53*, 2615–2619.
- (70) Sun, Q.; Aguila, B.; Perman, J. A.; Nguyen, N. T.-K.; Ma, S. *J. Am. Chem. Soc.* **2016**, *138*, 15790–15796.
- (71) Gao, W.-Y.; Wojtas, L.; Ma, S. *Chem. Commun.* **2014**, *50*, 5316–5318.
- (72) Kumar, S.; Verma, G.; Gao, W.-Y.; Niu, Z.; Wojtas, L.; Ma, S. *Eur. J. Inorg. Chem.* **2016**, *2016*, 4373–4377.